

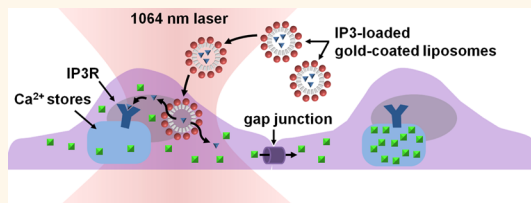


# Focal Activation of Cells by Plasmon Resonance Assisted Optical Injection of Signaling Molecules

Gabriel V. Orsinger,<sup>†</sup> Joshua D. Williams,<sup>†,‡</sup> and Marek Romanowski<sup>†,\*</sup>

<sup>†</sup>Department of Biomedical Engineering, University of Arizona, 1657 East Helen Street, Tucson, Arizona 85721, United States, and <sup>‡</sup>The University of Arizona Cancer Center, University of Arizona, 1515 North Campbell Avenue, Tucson, Arizona 85724, United States

**ABSTRACT** Experimental methods for single cell intracellular delivery are essential for probing cell signaling dynamics within complex cellular networks, such as those making up the tumor microenvironment. Here, we show a quantitative and general method of interrogation of signaling pathways. We applied highly focused near-infrared laser light to optically inject gold-coated liposomes encapsulating bioactive molecules into single cells for focal activation of cell signaling. For this demonstration, we encapsulated either inositol trisphosphate (IP3), an endogenous cell signaling second messenger, or adenophostin A (AdA), a potent analogue of IP, within 100 nm gold-coated liposomes, and injected these gold-coated liposomes and their contents into the cytosol of single ovarian carcinoma cells to initiate calcium ( $\text{Ca}^{2+}$ ) release from intracellular stores. Upon optical injection of IP3 or AdA at doses above the activation threshold, we observed increases in cytosolic  $\text{Ca}^{2+}$  concentration within the injected cell initiating the propagation of a  $\text{Ca}^{2+}$  wave throughout nearby cells. As confirmed by octanol-induced inhibition, the intercellular  $\text{Ca}^{2+}$  wave traveled via gap junctions. Optical injection of gold-coated liposomes represents a quantitative method of focal activation of signaling cascades of broad interest in biomedical research.



**KEYWORDS:** focal activation · optical trap · liposomes · gold · nanoparticles · plasmon resonance · calcium signaling

Interactions among the cells that make up organs and various tissue types determine the function of living organisms in both the maintenance of healthy homeostasis and the development of disease. In cancer, dysfunctional and co-opted cell communication pathways have been linked to the development of drug resistances, metastasis, and increased recurrence.<sup>1</sup> Numerous interactions have been investigated including cross-talk between stromal and epithelial cell types,<sup>2</sup> localized enrichment of endocrine and growth factor signaling within cell populations,<sup>3</sup> and alterations cell-matrix associations observed in epithelial-mesenchymal transition.<sup>4</sup> Further, experimental evidence and clinical observations have converged in support of the view that the complex, and often highly heterogeneous, tumor microenvironment actively participates in all phases of cancer development.<sup>5</sup> It is this heterogeneity and complexity that demands the development of new experimental techniques that enable identification and manipulation of biological communication pathways starting at a single cell level.<sup>6</sup>

Focal activation of a single cell in a quantitative manner remains a particularly challenging task. The prevailing method of mechanical stimulation does not account for complexities of many communication pathways, and necessitates new methods for precise delivery of messenger molecules to study of various stages of diverse signal cascades.<sup>7</sup> For quantifiable delivery of a broad range of unmodified bioactive molecules to a single cell, nanoparticle- and laser-assisted intracellular delivery techniques are being explored. For example, infrared (IR) laser light can manipulate sub-100 nm lipid vesicles with high refractive index cores, achieved by encapsulating 1 M sucrose, yielding an inducible dipole moment suitable for stable optical trapping.<sup>8</sup> Sub-100 nm metallic particles also efficiently interact with IR optical trapping lasers due to their high polarizability and can be optically injected across lipid membranes to transiently open 100 to 200 nm pores.<sup>9</sup> This process relies on simultaneous plasmonic heating and optical force in the direction of light propagation to push the

\* Address correspondence to marekrom@email.arizona.edu.

Received for review March 21, 2014 and accepted May 30, 2014.

Published online May 30, 2014  
10.1021/nn5015903

© 2014 American Chemical Society

gold nanoparticle through the lipid membrane, leaving a perforation that allows diffusion of extracellular solutes into the cell. Similarly to optical transfection methods, using laser light alone can perforate a cell membrane and allow internalization of nucleic acids.<sup>10</sup> There is, however, no broad method for quantifiable delivery of many types of molecular agents that targets only the single cell of interest while retaining cell viability.

We previously introduced light-sensitive gold-coated liposome for encapsulation and controlled delivery of soluble drugs and contrast agents, as a platform system for therapeutic and diagnostic delivery.<sup>11</sup> Morphology of this composite nanocapsules was elucidated by electron microscopy observations, and their optical properties described by applying the effective medium theory, as summarized elsewhere.<sup>12</sup> Gold-coated liposomes selectively absorb visible to NIR light, providing a photothermal trigger for rapid content release.<sup>13,14</sup> We have employed gold-coated liposomes for the localized extracellular delivery of active G-protein coupled receptor (GPCRs) agonists.<sup>15</sup> The strong polarizability of the gold shell surrounding the liposome's lipid membrane enhances optical trapping and facilitates the optical injection of these nanocarriers into cells. We then demonstrated intracellular delivery by optical injection of gold-coated liposomes encapsulating TO-PRO-3, a cell-impermeant fluorescent nuclear dye, while maintaining viability of cells following optical injection.<sup>16</sup>

Here, we introduce the method of focal activation of intercellular communication by optical injection of gold-coated liposomes. We applied a modulated optical trap to propel, or optically inject, 100 nm gold-coated liposomes encapsulating signaling molecules into a single cell. The number of gold-coated liposomes delivered into the single cell was determined by incorporation of a fluorescently-tagged lipid within the liposomes, allowing quantification of the dose of active molecules delivered into the cytosol. As a demonstration of focal activation, we examined intercellular calcium ( $\text{Ca}^{2+}$ ) signaling in the ovarian carcinoma cell line OVCAR-3, initiated by precise delivery of inositol trisphosphate (IP3) or adenophostin A (AdA) encapsulated within gold-coated liposomes. IP3 (Figure 1a) is a ubiquitous secondary messenger in GPCR and receptor tyrosine kinase (Rtk) signaling pathways, acting as an agonist of intracellular IP3 receptors (IP3Rs) leading to intracellular  $\text{Ca}^{2+}$  release.<sup>17–20</sup> AdA (Figure 1b), an analogue of IP3 with greater affinity for IP3Rs, has been shown to exhibit a half maximal effective concentration ( $\text{EC}_{50}$ ) of 8.3 nM for IP3R subtype 1 versus IP3's  $\text{EC}_{50}$  of 87 nM for the same receptor.<sup>21</sup> Increases in cytosolic  $[\text{Ca}^{2+}]$  elicited by delivery of liposomal IP3 or AdA were monitored in the single injected cell and neighboring cells using the  $\text{Ca}^{2+}$ -sensitive fluorescent dye Indo-1.<sup>22</sup> This application of optical injection represents a new,

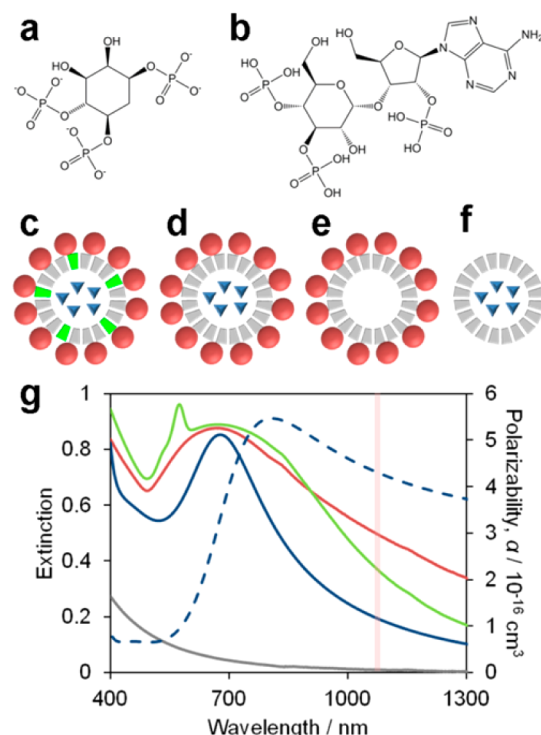


**Figure 1. Liposome formulations and associated extinction spectra.** Molecular structures of (a) IP3 and (b) AdA. Schematic of (c) fluorescently tagged IP3-loaded gold-coated liposomes, (d) IP3- or AdA-loaded gold-coated liposomes, (e) blank gold-coated liposomes, and (f) IP3-loaded uncoated liposomes. (g) Extinction spectra of IP3-loaded gold-coated liposomes made with 0.05 mol % DPPE-RhB (green line, corresponding to (c)), IP3-loaded gold-coated liposomes (red line, corresponding to (d) and (e)), and IP3-loaded uncoated liposomes (gray line, corresponding to (f)). Computationally derived extinction spectrum (solid blue line) and polarizability (dashed blue line) based on 100 nm diameter gold-coated liposomes with 2 nm gold shell at a fill factor 0.76.

quantitative method of focal activation of signaling cascades of broad interest in biomedical research, free of many limitations of currently used techniques such as mechanical stimulation or photouncaging.

## RESULTS

**Spectral Properties of Liposomes.** A total of five liposome formulations were prepared. First, to quantify the delivery of gold-coated liposomes by optical injection, liposomes encapsulating 500  $\mu\text{M}$  IP3 in phosphate buffered saline (PBS) were prepared incorporating 0.05 mol % of rhodamine-B (RhB) conjugated lipid and gold coated (Figure 1c). For initiating  $\text{Ca}^{2+}$  signaling, two liposome formulations were prepared encapsulating either 500  $\mu\text{M}$  IP3 or 50  $\mu\text{M}$  AdA in PBS and gold coated (Figure 1d). To assess the effect of injecting gold-coated liposomes into cells without the presence of signaling molecules, a fourth formulation of liposomes was prepared without IP3 or AdA and gold coated (Figure 1e). As the fifth formulation, a portion of the 500  $\mu\text{M}$  IP3-loaded liposomes were left uncoated to serve as the negative control (Figure 1f). Liposomes

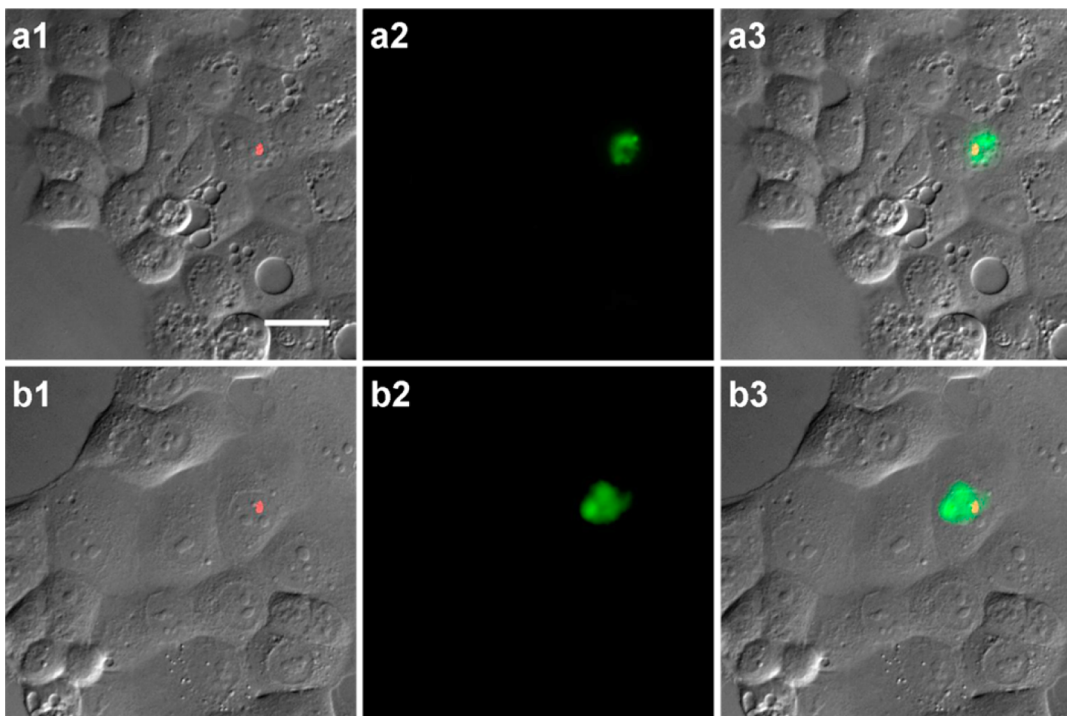


**Figure 2.** Optical injection of fluorescently tagged gold-coated liposomes. The panel shows the accumulation of RhB-tagged gold-coated liposomes (shown in green) delivered *via* optical injection for a duration of 60 s (row a) and 120 s (row b). Column 1 is the experimental field of view (FOV) of OVCAR-3 cells in differential interference contrast (DIC) with the location of the optical injecting laser overlaid in red. Column 2 shows the resulting RhB fluorescence signal after 60 or 120 s of optical injection. Column 3 is the merged image of columns 1 and 2 showing localization of the fluorescent signal with the position of the laser. Scale bar = 25  $\mu\text{m}$ , all images.

had an average diameter of 95–100 nm (number-weighted) prior to gold coating, and 100–105 nm following the gold coating process as determined by dynamic light scattering. Gold-coated liposomes (Figure 1d,e) exhibited peak plasmon resonances around 700 nm (Figure 1g, red line). A similar spectrum was observed for RhB-labeled gold-coated liposomes (Figure 1c) with an additional peak around 570 nm corresponding to RhB absorption. A computationally derived extinction spectrum (Figure 1g, solid blue line) for 100 nm diameter gold-coated liposomes with 2 nm gold shell at a fill factor of 0.76 shows a peak resonance at 700 nm. Similarly calculated polarizability of these gold-coated liposomes (Figure 1g, dashed blue line) is  $4.24 \times 10^{-16} \text{ cm}^3$  at 1064 nm (Figure 1g, vertical line) and is responsible for the gradient force in the highly focused 1064 nm laser beam.<sup>16</sup> As expected, uncoated liposomes (Figure 1f) exhibited no plasmon resonance (Figure 1g, gray line).

**Quantification of Gold-Coated Liposome Optical Injection.** Under the settings described in Methods, the average power of the optical injection beam in the plane of sample was 10 mW. Optical injection of gold-coated liposomes prepared with 0.05 mol % DPPE-RhB resulted in RhB fluorescence localized within the injected cell, whereas the intensity of fluorescence relates to the duration of optical injection (Figure 2).

Analysis of the intensity of fluorescence originating from a single cell enabled us to establish a quantitative

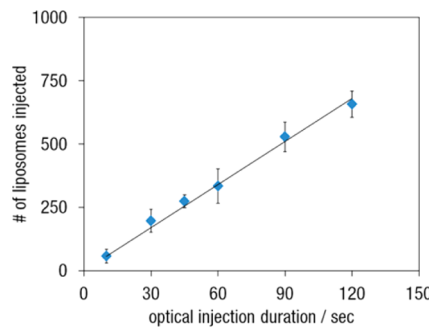


**Figure 3.** Quantitative optical injection of liposomes. The plot shows the linear relationship between optical injection duration and the number of liposomes delivered to the injected cell. For each point,  $n = 3$ , mean  $\pm$  standard deviation.

relation between the injection time and the number of cargo-carrying liposomes delivered to the cytoplasm. We calculated the number of injected liposomes by dividing the integrated intensity of fluorescence emitted by an injected cell by that originating from a single liposome (see Methods for details). Figure 3 plots the calculated number of liposomes optically injected into single cells for durations of 10, 30, 45, 60, 90, and 120 s at a constant lipid concentration of 10 mM (approximately  $6 \times 10^{10}$  liposomes/ $\mu\text{L}$ ) and the optical injection laser settings described in Methods. Linear regression analysis of the data ( $R^2$  value of 0.992)

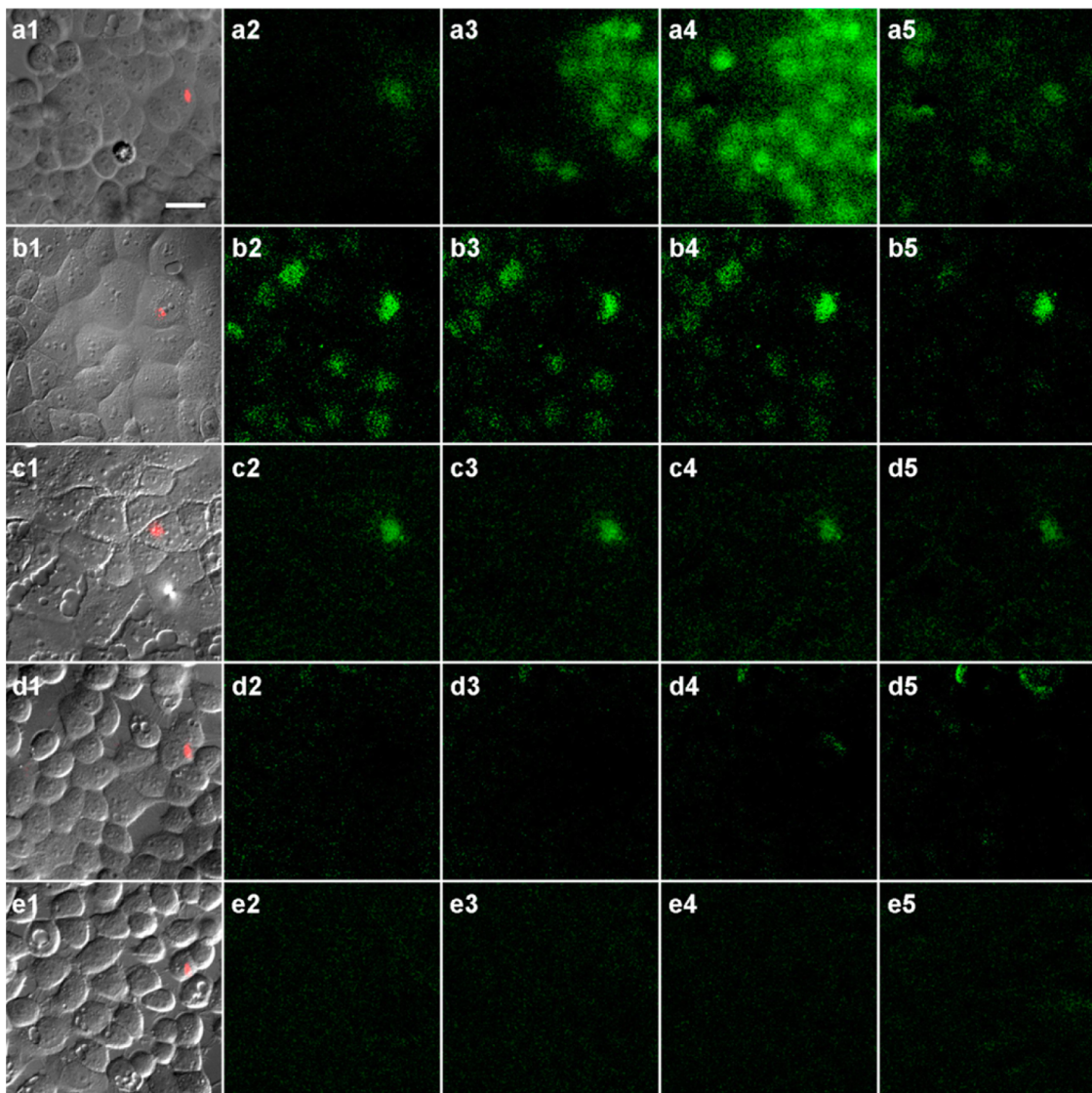


**Figure 4.**  $\text{Ca}^{2+}$  signal propagation in OVCAR-3 cells in response to optical injection. Representative examples of five experimental conditions are shown: (a) optical injection of gold-coated liposomes encapsulating IP3; (b) optical injection of gold-coated liposomes encapsulating AdA; (c) optical injection of gold-coated liposomes encapsulating IP3 in cells treated with octanol; (d) optical injection of gold-coated liposomes containing PBS but no signaling molecules. (e) Attempt to optically inject uncoated liposomes encapsulating IP3. Column 1 shows the experimental FOV in DIC merged with the laser spot. Columns 2–5 show calculated  $\text{Ca}^{2+}$  signal over baseline, as reported by Indo-1 fluorescence, at 45, 60, 75, and 120 s after initiation of optical injection. Movies corresponding to images are in Supporting Information, S1–S5. Bar = 25  $\mu\text{m}$ , applies to all panels.

indicates that the gold-coated liposomes are injected at the rate of  $5.7 \text{ s}^{-1}$  throughout the tested range of injection times, up to 120 s.

To estimate the number of *signaling molecules* delivered to the cytoplasm in this process, we assumed that the dose of encapsulated molecules delivered to the cell was proportional to the number of injected liposomes, in the manner dependent on the concentration of encapsulated content. For example, at the IP3 concentration of  $500 \mu\text{M}$ , each 100 nm diameter liposome encapsulates approximately 120 IP3 molecules.  $\text{Ca}^{2+}$  release from the endoplasmic reticulum requires a minimum concentration of 30 nM of the cellular IP3,<sup>23</sup> a level normally activated by upstream agonists to

extracellular GPCR or Rtk receptors. To reach the minimum activating concentration of 30 nM IP3, at least 77 liposomes must be delivered into the typical cell volume of  $0.5 \times 10^{-12} \text{ L}$ . The calibration data obtained using fluorescently tagged gold-coated liposomes (Figure 3) indicates that this threshold is met at approximately 14 s into optical injection.

**Optical Injection of Gold-Coated Liposomes Encapsulating Signaling Molecules.** We monitored intracellular  $[\text{Ca}^{2+}]$  changes induced by delivery of IP3 or AdA carried by optically injected gold-coated liposomes. The resulting fluctuations in  $[\text{Ca}^{2+}] / [\text{Ca}^{2+}]_{\text{baseline}}$  are determined as the ratio of Indo-1 fluorescence intensity over baseline fluorescence and shown in Figure 4. Column 1 of

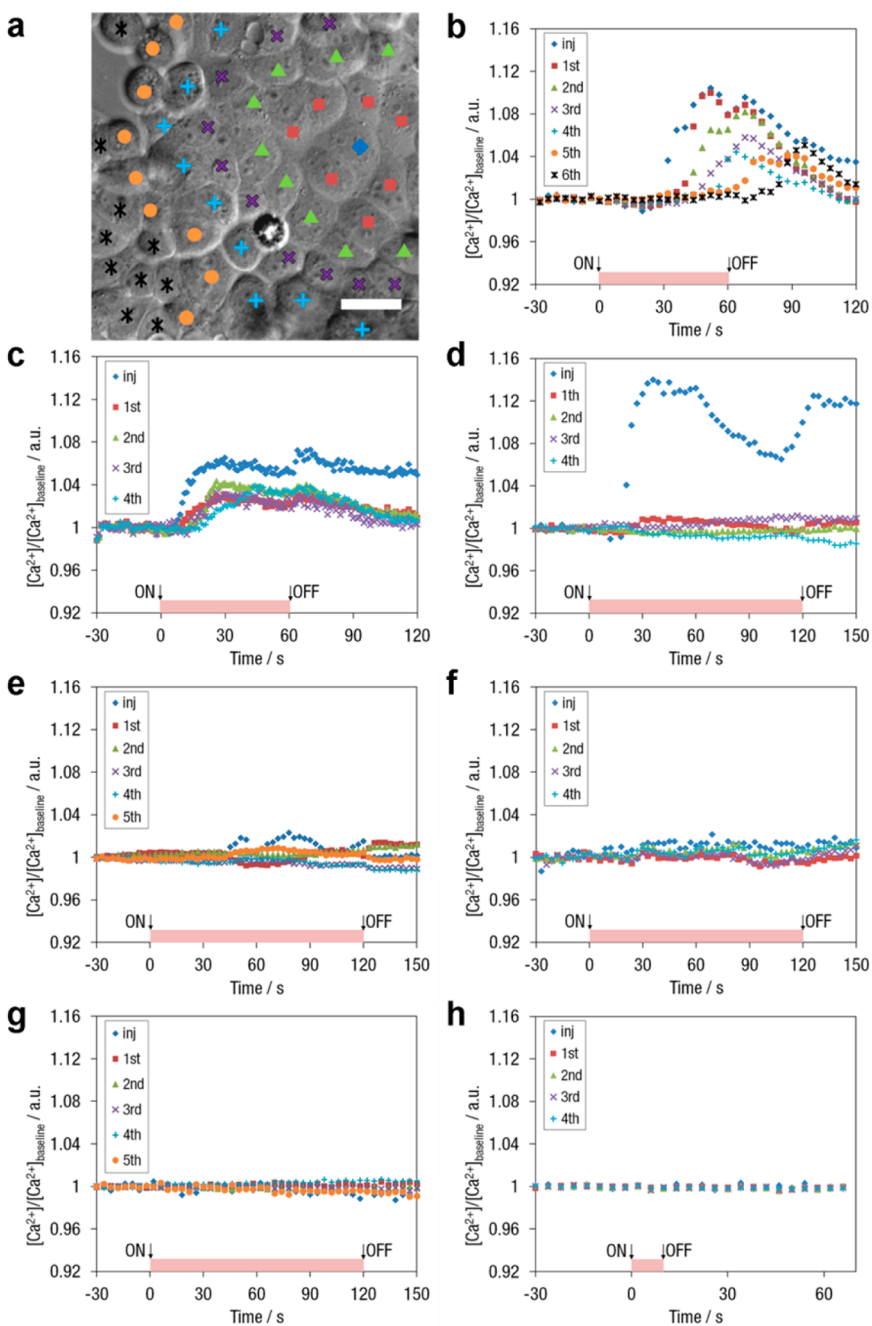


**Figure 5.**  $\text{Ca}^{2+}$  signal propagation grouped by degrees of separation from single activated cell. (a) Cells were grouped by degrees of separation spanning outward from injected cell (blue ♦) as marked on the example DIC image of OVCAR-3 cells: first group (red ■), second group (green ▲), third group (violet ×), fourth group (teal +), fifth group (orange ●), and sixth group (black \*). Bar = 25  $\mu\text{m}$ . (b) Gold-coated liposomes encapsulating 500  $\mu\text{M}$  IP3 optically injected for 60 s resulted in a sequentially-spreading  $\text{Ca}^{2+}$  signal in OVCAR-3 cells. (c) Gold-coated liposomes encapsulating 50  $\mu\text{M}$  AdA optically injected for 60 s also resulted in a sequentially-spreading  $\text{Ca}^{2+}$  signal. (d) OVCAR-3 cells treated with 1 mM octanol showed a  $\text{Ca}^{2+}$  signal localized to only the injected cell. (e) Gold-coated liposomes containing PBS but no signaling molecules optically injected for 120 s showed only a minimal increase in  $[\text{Ca}^{2+}]$  at the injected cell. (f) Uncoated IP3-loaded liposomes optically injected for 120 s resulted in no detectable  $\text{Ca}^{2+}$  response. (g) Exposure to the 1064 nm trapping laser to a single cell in the absence of liposomes for 120 s resulted in no detectable  $\text{Ca}^{2+}$  signal. (h) Gold-coated liposomes encapsulating 500  $\mu\text{M}$  IP3 injected for 10 s resulted in no observable  $\text{Ca}^{2+}$  signal. Data points represent average change in Indo-1 fluorescence intensity over baseline fluorescence intensity per group of cells.

Figure 4 shows differential interference contrast (DIC) images of the experimental field of view (FOV) merged with an image of the optical trap focal spot, which indicates the cell selected for optical injection. The increases in the ratio of  $[\text{Ca}^{2+}]/[\text{Ca}^{2+}]_{\text{baseline}}$  at 45, 60,

75, and 120 s after initiation of optical injection are shown in Figure 4 columns 2, 3, 4, and 5, respectively. These results are also summarized in Figure 5 as plots of  $[\text{Ca}^{2+}]/[\text{Ca}^{2+}]_{\text{baseline}}$  versus time for the optically injected cell and neighboring cells grouped by degrees

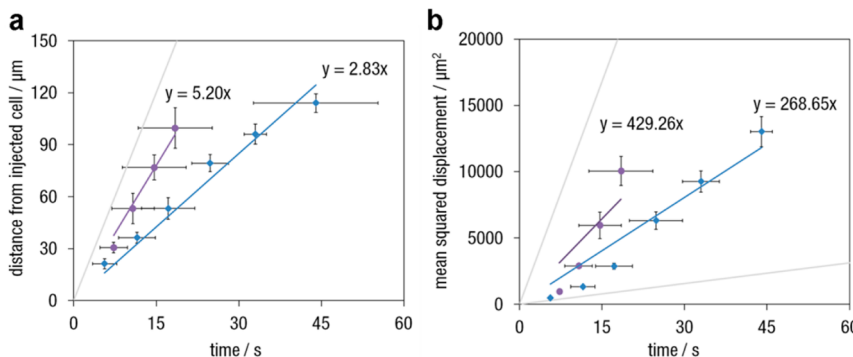


**Figure 6.** (a) Timing of intercellular  $\text{Ca}^{2+}$  signal, grouped by degrees of separation, traveling outward from an optically injected cell activated by IP3-encapsulating gold-coated liposomes (blue  $\blacklozenge$ ) and AdA-encapsulating gold-coated liposomes (violet  $\bullet$ ). Shown for comparison, intercellular  $\text{Ca}^{2+}$  waves travel an average of  $8 \mu\text{m/s}$  (gray line) in thymic epithelial cells.<sup>25</sup> (b) Mean squared displacement of the same  $\text{Ca}^{2+}$  signals over time. Mean squared displacement of free cytosolic  $\text{Ca}^{2+}$  and IP3 (gray lines) are also plotted, calculated from published diffusion coefficients for cytosolic  $\text{Ca}^{2+}$ ,  $0.13 \times 10^{-6} \text{ cm}^2/\text{s}$ , and for cytosolic IP3,  $2.8 \times 10^{-6} \text{ cm}^2/\text{s}$ .<sup>7</sup>

of separation from the single injected cell. All cells in direct contact with the injected cell comprised the first group, all cells in direct contact with the first group comprised the second group, and so on, with each group of cells including those in direct contact with the previous group. An example of this scheme for grouping cell is depicted in Figure 5a.

Optical injection of gold-coated liposomes encapsulating  $500 \mu\text{M}$  IP3 into a single OVCAR-3 cell for 60 s, providing an intracellular concentration of approximately 120 nM, resulted in widespread  $\text{Ca}^{2+}$  signaling within the FOV beginning at the injected cell and sequentially spreading outward to the neighboring cell groups (Figures 4a1–a5 and 5b, and Supporting Information Movie S1). The observed  $\text{Ca}^{2+}$  signal begins at the injected cell 30 s into optical injection, spreads sequentially by degree of separation to all cells in the experimental FOV, then returns to near baseline at 120 s (60 s after optical injection turned off).

For comparison, we tested AdA, a highly potent agonist of IP3Rs shown to have 10 times greater affinity for IP3Rs than IP3.<sup>21</sup> Optical injection of gold-coated liposomes encapsulating  $50 \mu\text{M}$  AdA into OVCAR-3 cells for 60 s, yielding an estimated intracellular AdA concentration of 12 nM, similarly resulted in widespread and sequential  $\text{Ca}^{2+}$  signaling (Figures 4b1–b5 and 5c, and Supporting Information Movie S2). Rapid onset of  $\text{Ca}^{2+}$  signaling at the cell injected with liposomal AdA is observed at around 15 s.

Pretreating the OVCAR-3 cells with 1 mM octanol, a known blocker of gap junctions,<sup>24</sup> effectively confined the observed  $[\text{Ca}^{2+}]$  changes to only the single cell optically injected with gold-coated liposomes encapsulating  $500 \mu\text{M}$  IP3, with no evidence of  $[\text{Ca}^{2+}]$  changes in adjacent cells, even after 120 s of continuous injection delivering an approximate dose of 240 nM IP3 to the cell (Figures 4c1–c5 and 5d, and Supporting Information Movie S3).

Negative control experiments showed negligible changes in cytosolic  $[\text{Ca}^{2+}]$ . The first control, in which gold-coated liposomes without IP3 were injected, showed only a 2% increase in Indo-1 fluorescence intensity over baseline at the injected cell observed at 75 s into injection and no propagation to surrounding cells (Figures 4d1–d5 and 5e, and Supporting Information Movie S4). Additional attempts to optically inject IP3-loaded liposomes without the gold coating for 120 s consistently showed no observable  $\text{Ca}^{2+}$  response (Figures 4e1–e5 and 5f, and Supporting Information Movie S5). Exposing a single cell to the trapping laser alone for up to 120 s in the absence of liposomes also failed to induce observable changes in Indo-1 fluorescence in either the single cell exposed to the optical injection beam or the surrounding cells (Figure 5g, and Supporting Information Movie S6). No  $\text{Ca}^{2+}$  signal was observed in response to delivery of a subthreshold dose of IP3, as demonstrated by 10 s of optical injection of gold-coated liposomes encapsulating  $500 \mu\text{M}$  IP3 which resulted in a cytosolic IP3 concentration of approximately 20 nM (Figure 5h, and Supporting Information Movie S7).

**Propagation of  $\text{Ca}^{2+}$  Signal.** To illustrate how the proposed method of focal activation can aid quantitative analysis of cellular environment, we examined propagation of  $\text{Ca}^{2+}$  signal. The timing of the  $\text{Ca}^{2+}$  signal propagation throughout the cells can be used to calculate the velocity of the  $\text{Ca}^{2+}$  signal or, alternatively, the apparent diffusion coefficient responsible for the spread of observed signal. Figure 6a shows distance of  $\text{Ca}^{2+}$  signal traveling away from the injected cell plotted against time as grouped by degrees of separation for OVCAR-3 cells activated by IP3- and AdA-encapsulating gold-coated liposomes. The slope of the linear regression fit to these data reveals the velocity of IP3-induced  $\text{Ca}^{2+}$  signaling as  $2.83 \mu\text{m/s}$  and of AdA-induced  $\text{Ca}^{2+}$  signaling as  $5.20 \mu\text{m/s}$ .

Alternatively, the wavelike nature of  $\text{Ca}^{2+}$  signal propagation throughout gap-junction linked cells can

be described using the apparent diffusion coefficient associated with the observed signal. When we plot the mean squared displacement of the outward spreading  $\text{Ca}^{2+}$  signal *versus* time, the apparent diffusion coefficient in two-dimensional space can be estimated from linear regression analysis of the relation:

$$\langle x^2 \rangle = 4Dt$$

where  $\langle x^2 \rangle$  is the mean squared displacement,  $D$  is the diffusion coefficient, and  $t$  is time. Figure 6 shows the analysis of the mean squared displacement of IP3- and AdA-induced  $\text{Ca}^{2+}$  signaling obtained from the experimental results shown in Figures 4a and 5b for IP3 and Figures 4b and 5c for AdA. These data reveal apparent diffusion coefficients of  $0.67 \times 10^{-6}$  and  $1.07 \times 10^{-6} \text{ cm}^2/\text{s}$  for IP3- and AdA-induced intercellular signaling, respectively.

## DISCUSSION

Here, we demonstrated the versatility, control, and quantitative nature of focal cellular activation by optical injection of gold-coated liposomes. Perhaps most frequently focal activation is achieved by gentle mechanical stimulation of a cell with a micropipet or similar means, which then triggers production of IP3.<sup>26,27</sup> While mechanical stimulation is relevant to certain, mechanosensitive cells, the overall diversity of signal transduction pathways demands appropriately versatile methods of focal activation. In particular, arbitrary control of intracellular concentrations of various messenger molecules may enable investigation of specific stages of many signal transduction pathways of interest to biomedical researchers. Local delivery of molecular agents to single cells can be achieved by microinjection,<sup>28,29</sup> optoporation,<sup>30,31</sup> and photolysis of chemically modified agonists or photouncaging.<sup>32–35</sup> Each of these methods carries inherent technical limitations. For example, while microinjection allows quantitative delivery of molecules to a single cell in small volumes, micropipet contact can easily result in cell damage and unintentional mechanical stimulation of cell signaling, masking specific cellular responses to agonists. Optoporation techniques, either enabled by light absorbing membrane dyes or femtosecond lasers, transiently open a cell's membrane for passive diffusion of extracellular molecules into that cell. Smallest pore sizes are determined by the diffraction limited laser spot size, typically hundreds of nanometers, and have been shown to persist around 20 s.<sup>36</sup> With these and other membrane perforation techniques,<sup>9</sup> the dose of active molecules and the rate of delivery is dependent on large extracellular concentrations and, generally unknown, kinetics of that process. Realizations of such experimental techniques in the context of cell signaling are further complicated by the possible influx of  $\text{Ca}^{2+}$  or signaling agents from the extracellular space, and release of ATP and other cellular components from the cytosol.

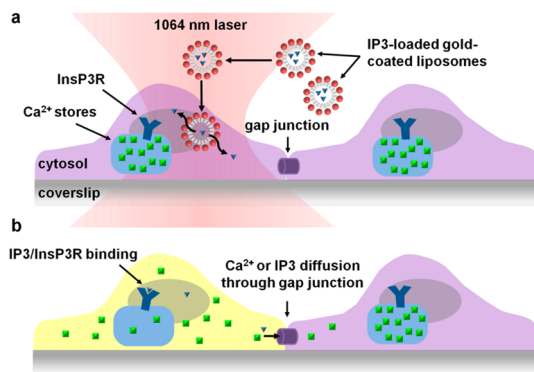


**Figure 7.** Proposed mechanism of inducing intercellular  $\text{Ca}^{2+}$  signaling by optical injection of gold-coated liposomes encapsulating IP3. (a) Freely diffusing gold-coated liposomes encapsulating IP3 encounter the 1064 nm laser beam and are propelled toward the cell. Optically injected into a single cell, they move toward the focal point of the trap (shown as the beam waist) where IP3 molecules (blue triangles) are released into the cytosol. (b) IP3 binds to the intracellular IP3R, initiating rapid release of stored  $\text{Ca}^{2+}$  (green squares) into the cytosol.  $\text{Ca}^{2+}$  and/or IP3 are then able to diffuse through the gap junctions to induce rapid release of stored  $\text{Ca}^{2+}$  into the cytosol of adjoining cells.

Alternatively, photouncaging techniques provide high temporal and spatial resolutions of delivery; however, they rely on chemical compounds not designed to cross the cellular membrane and therefore require preloading in the cell, possibly by microinjection or optoporation. Molecules for photouncaging techniques must be chemically modifiable, so types of signaling molecules amenable to this technique are limited. Given the complexity of multistep syntheses, applicability of photouncaging in biomedical laboratories is typically limited to compounds available commercially.<sup>35</sup>

The optical injection of gold-coated liposomes process that we report here addresses many of these challenges. In this technique, the focal spot of the optical trap is purposefully placed within the targeted cell. In this manner, we create an optical force field capable of accelerating nanoparticles in the manner dependent on their polarizability. Gold-coated liposomes diffuse freely in the extracellular space and, once they encounter the optical force field, are propelled toward the focal point of the trap. Moving toward the focal point, they are exposed to increasing densities of electromagnetic field which in turn deposit increasing amount of heat, eventually resulting in thermal destabilization and content release (Figure 7a). Notably, content release in this setting does not require any specific activation by the operator of the optical trap, rather it is an inevitable consequence of the gold-coated liposomes propelled to its own demise.

The gold-coated liposomes used for this experimental work were specifically made with peak plasmon resonance around 700 nm, well below the 1064 nm wavelength of trapping beam, to reduce absorption of light by these liposomes (40% of its value at maximum,

Figure 1g) and subsequent thermal damage and premature leakage of content. However, at 1064 nm these gold-coated liposomes retain significant polarizability (80% of its maximal value, Figure 1g), resulting in greater optical forces and ability to steer the liposomes toward the cell.

Our proposed mechanism of delivery into the cell's cytosol involves two events, breaching the cell membrane followed by disruption of the gold-coated liposomes structural integrity. Experimental separation of these two events remains challenging, although we show that photoporation is not involved there. Exposing a single cell to the trapping laser for 2 min without gold-coated liposomes in the extracellular medium resulted in no detectable decrease in Indo-1 fluorescence (Figure 5g), indicating that the integrity of the cellular membrane was maintained. A perforated cell would rapidly lose Indo-1 molecules to the extracellular medium. This agrees with our earlier optical injection work that demonstrated laser trap does not compromise integrity of the cell membrane.<sup>16</sup>

Liposomal encapsulation is applicable to a broad class of water-soluble factors, including exogenous probes such as TO-PRO-3, previously demonstrated by our group,<sup>16</sup> or second messengers, exemplified here using IP3 and its analogue AdA. We selected activation of IP3R for this demonstration as this represents one of many biological processes deregulated in cancer.<sup>37</sup> Different research groups have shown that IP3R is the target of proto-oncogenes, such as protein kinase B,<sup>38</sup> and tumor suppressors, for example pro-myelocytic leukemia protein.<sup>39</sup> Precise intracellular delivery of IP3 and its potent analogues described here may aid in studying deregulated properties of cancer cells and mapping altered signaling networks. Liposomal encapsulation is performed with no chemical modification, leaving no residual background activity of the molecule, which is a frequent problem accompanying caging of biological molecules. Delivery and release can be performed in a quantitative manner, and it is possible to adjust gold-coated liposome or encapsulated solute concentrations to fine-tune the rate and quantity of delivered compound in a very broad range. At the 10 mM lipid and 500 μM IP3 concentrations used here, we typically required 30 s of injection to activate Ca<sup>2+</sup> signaling. Conceivably, liposomes can be prepared at 60 mM lipid and 120 mM IP3 concentration (the maximum IP3 solubility in PBS). At this upper limit, an above-threshold intracellular IP3 concentration of 95 nM can be achieved within 30 ms of injection. For attenuated and more precise delivery, gold-coated liposomes prepared encapsulating 4 μM IP3 (resulting in approximately 1 IP3 molecule per liposome) diluted to an effective 100 μM lipid concentration can be used to count and deliver single IP3 molecules into the cell. In this model, we make the assumption that the number of liposomes optically

injected deliver the entire payload of encapsulated IP3; however, in the case that there is premature leakage of encapsulated IP3 prior to cellular entry, the amount delivered may be less.

Focal activation of cells by optical injection of gold-coated liposomes enables quantitative analysis of the resulting intercellular Ca<sup>2+</sup> wave. As demonstrated in Figure 6a, plotting the time course of the wave propagation reveals signaling velocities of 2.83 and 5.20 μm/s in response to IP3 and AdA injections, respectively. For comparison, intercellular Ca<sup>2+</sup> waves are typically reported to travel between 10 and 20 μm/s,<sup>7</sup> and 8 μm/s for thymic epithelial cells.<sup>25</sup> We also demonstrated that this method can be used to measure the apparent diffusion coefficient of intercellular Ca<sup>2+</sup> signaling. We calculated this to be  $0.67 \times 10^{-6}$  and  $1.07 \times 10^{-6}$  cm<sup>2</sup>/s in response to delivery of IP3 and AdA, respectively, values that are within the range of published diffusions coefficients for intracellular Ca<sup>2+</sup>,  $0.13 \times 10^{-6}$  cm<sup>2</sup>/s and cytosolic IP3,  $2.8 \times 10^{-6}$  cm<sup>2</sup>/s (Figure 6b).<sup>7</sup>

Optical injection of gold-coated liposomes described here combines both controlled *delivery* and *release* of molecules of interest. In comparison, recent works from several laboratories explain how plasmon resonant nanoparticles illuminated with laser light can initiate intracellular release of a drug, nucleic acid, or fluorescent probes once associated carriers are delivered to cells by molecular targeting or nonspecific endocytosis.<sup>40–42</sup> Similarly, efficient photothermal conversion in liposome-embedded indocyanine green, a near-infrared molecular dye, can be used to trigger intracellular release of the contents of such liposomes taken by a cell via endocytosis.<sup>43</sup> However, all these methods require some other, efficient mechanism of cellular entry, either nonspecific or based on activity of a specific molecular marker triggering cellular entry. Moreover, none of these methods enable addressing individual cells in their microenvironment. Free of these limitations, optical injection of gold-coated liposomes is well suited for studying phenotypic heterogeneity of cells, independent of varying patterns of expression of molecular markers in the cell membrane. As cell populations actually can behave in a functional heterogeneous manner,<sup>44,45</sup> the ability to interrogate a single cell with bioactive agents and subsequently monitor the response facilitates a better understanding of phenotypic variations within cell populations.

Quantitative focal activation can also find applications in interrogating cell communication pathways in multicompartmental models of the tumor microenvironment, such as co-cultured or 3D models. In one illustrative example, optical injection of gold-coated liposomes encapsulating 500 μM IP3 was applied to interrogate Ca<sup>2+</sup> signaling in a co-cultured model of OVCAR-3 ovarian carcinoma cells in direct contact with supportive fibroblasts (Figure 8, and Supporting Information Movie S8). Propagation of Ca<sup>2+</sup> signaling was

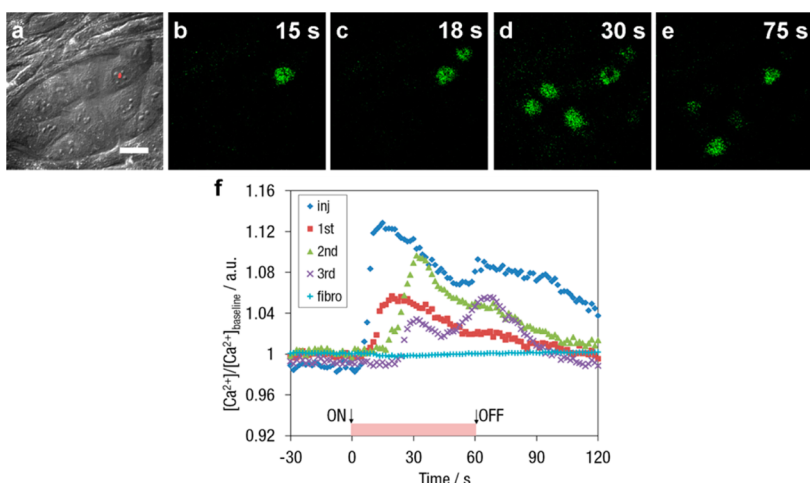


**Figure 8.** Optical injection in a co-culture of epithelial and stromal cells. (a) DIC of OVCAR-3 cells grown in a cluster encircled by Hs-27 fibroblasts merged with the location of optical injecting laser. (b)  $\text{Ca}^{2+}$  signaling at 15 s after the onset of optical injection, (c) 18 s, (d) 30 s, and (e) 75 s. (f) The plotted  $\text{Ca}^{2+}$  response shows widespread signaling localized to the cluster of OVCAR-3 cells with no cross talk to fibroblasts. Movie corresponding to images found in Supporting Information, S8. Bar = 25  $\mu\text{m}$ , applies to (a–e).

confined to the island of OVCAR-3 cells and did not spread into the surround fibroblasts, indicating gap-junction coupling among OVCAR-3 cells but not between OVCAR-3 and fibroblast cell types, as expected due to limited presence of direct communication pathways between these physiologically separate cell types.<sup>46</sup>

## CONCLUSIONS

We have demonstrated quantitative focal activation of individual cells by the use of optical manipulation to gold-coated liposomes. Specifically, we demonstrated how this quantitative focal activation may be used to determine parameters of cellular communication. Because encapsulated molecules require no chemical modification, we believe this method of

quantitative intracellular delivery can be applied universally to any water-soluble molecules, while maintaining diffraction limited spatial resolution in combination with doses (zeptomoles) and volumes (attoliters) unattainable by traditional microinjection and photouncaging techniques. Optical injection of gold-coated liposomes may enable the study of single cell dose-response curves for delivery of therapeutics and potentially elucidate functional heterogeneity of cells within a normal tissue or a tumor microenvironment. A better understanding of complex signaling networks beginning at a single cell level, facilitated by the novel experimental method of optical injection of gold-coated liposomes, could lead to improved therapies and diagnostics.

## METHODS

**Preparation of Gold-Coated Liposomes.** Five formulations of thermosensitive liposomes were prepared from synthetic lipids similar to a composition previously demonstrated for temperature-sensitive content release.<sup>47</sup> The general formulation consisted of dipalmitoylphosphatidylcholine (DPPC), monopalmitoylphosphatidylcholine (MPPC), and dipalmitoylphosphatidylethanolamine-N-[methoxy(polyethylene glycol)-2000] (DPPE-PEG2000) (Avanti Polar Lipids; Alabaster, AL) at a 90:10:4 molar ratio. The lipids were dissolved in chloroform, dried under nitrogen, and remaining solvent was removed under vacuum. Dried lipids were combined with PBS that included IP3 molecules to reach a lipid concentration of 60 mM. Liposomes were prepared by freeze-thaw cycling followed by extrusion through 100 nm porous polycarbonate membranes. Unencapsulated IP3 was removed via three rounds of dialysis using 100 000 molecular weight cutoff cellulose membranes (Spectrum Laboratories; Rancho Dominguez, CA). To form the plasmon resonant gold shell on the surface of the IP3-loaded liposomes, 18  $\mu\text{L}$  of 100 mM gold chloride was reduced by 27  $\mu\text{L}$  of 500 mM ascorbic acid in a 1 mL liposomal suspension at a 10 mM lipid concentration. This process is similar to the technique we previously reported.<sup>11</sup> A portion of the IP3-loaded liposomes was left uncoated for control experiments.

The first formulation of liposomes included 0.05 mol % dipalmitoylphosphatidylethanolamine-N-(lissamine rhodamine B sulfonyl) (DPPE-RhB) (Avanti Polar Lipids) with the other lipid components, encapsulated 500  $\mu\text{M}$  IP3 in PBS, and was gold coated. The second formulation of liposomes was prepared the same as the first formulation, but without DPPE-RhB. The third formulation was prepared similarly to the second, however, encapsulating 50  $\mu\text{M}$  AdA in PBS instead of IP3. The fourth formulation was prepared the same as the second and third, however, without including signaling molecules in the PBS. The fifth and final formulation of liposomes was aliquoted from the second formulation and was not gold coated.

The presence of the plasmon resonant structure was immediately evident by a change in suspension color, and the spectral position of peak plasmon resonance was determined via absorption spectra obtained on a Cary 5 spectrophotometer. Liposome size distributions were determined by dynamic light scattering (Zetasizer Nano ZS, Malvern Instruments Ltd., Worcestershire, U.K.).

**Cell Culture.** The majority of the experiments described here used OVCAR-3 cells (ATCC, Manassas, VA), a human epithelial ovarian cancer cell line. OVCAR-3 cells were subcultured under standard cell culture conditions in RPMI medium supplemented with 20% fetal bovine serum, 0.01 mg/mL bovine insulin, and

1% penicillin–streptomycin. For experimentation, near confluent cells from stock T-75 flasks were detached with 0.25% trypsin–EDTA and subcultured onto 18 mm round glass coverslips at a 1:5 split ratio and grown for 5 days in standard culture conditions prior to experimentation. OVCAR-3 cells used here were passage number 35–50.

For co-culture experiments, Hs-27 cells (ATCC), a human fibroblast cell line, were seeded at equal densities and grown with OVCAR-3 cells on glass coverslips under similar conditions. Dulbecco's Modified Eagle's Medium with 10% fetal bovine serum was mixed at a 1:1 ratio with the RPMI medium described above for co-culturing Hs-27 and OVCAR-3 cells.

**Optical Injection Setup.** The optical injection setup brings an optical trapping laser beam into an inverted microscope (IX71, Olympus, Center Valley, PA) and through a 60 $\times$  1.42 NA oil immersion lens (PLAPON 60XO, Olympus, Center Valley, PA) to create the highly focused optical trap. The trapping laser is a continuous wave 1064 nm TEM<sub>00</sub> Nd:YAG laser (Ventus IR, Laser Quantum, U.K.) with a 1.2 W maximum power, 1.2 M<sup>2</sup> value, and high beam pointing and power stability. Simultaneous optical injection and the ability to image cells in transmission DIC or by epi-fluorescence is enabled by a short pass VIS/IR beam splitter (T700dcsoxr-3p, Chroma, Bellows Falls, VT) adjacent to the objective, as depicted in Figure 9a. To modulate the trapping beam, we use a Pockels cell (360-80 LTA, Conoptics, Danbury, CT) controlled by a pulse generator (9530 Series Pulse Generator, Quantum Composers, Bozeman, MT) driving a voltage amplifier (25D Driver, Conoptics, Danbury, CT), used in combination with a Glan-laser polarizer. This light modulation system is capable of producing pulses as short as 20 ns and frequencies up to 30 MHz allowing for efficient trapping with little heat accumulation at the thermosensitive liposome.<sup>15</sup> For all optical injection experiments described here, the pulse generator was set to a pulse width of 500 ns and a frequency of 500 kHz (25% duty cycle). Prior to experimentation, the trapping beam's average power was measured after the 60 $\times$  objective. The position of the optical trap in the experimental FOV is controlled by two beam steering lenses ( $f = 250$  mm, Thorlabs, Newton, NJ) keeping one lens stationary and moving the other lens along the X-, Y-, and Z-axes with three motorized actuators. Samples were imaged onto an air-cooled 512  $\times$  512 pixel back-thinned electron-multiplying charge-coupled device (EMCCD) digital camera (Hamamatsu, Bridgewater, NJ) with a protective 1064 nm o.d. 6 rugate notch filter (Edmund Optics, Barrington, NJ) before the detector. DIC images were acquired via illumination by a 100 W tungsten halogen and epi-fluorescent images were acquired via illumination by a 200 W metal halide lamp (Lumen 220, Prior Scientific, Rockland, MA).

**Optically Injecting Fluorescent Liposomes.** Gold-coated liposomes containing 0.05 mol % DPPE-RhB lipids were used to quantify the rate of liposome delivery during the optical injection process. OVCAR-3 cells grown to confluence on a glass coverslip were washed in PBS and then assembled into a semiclosed cell chamber with two open ends. The assembled cell chamber consisted of a base coverslip adjacent to the oil immersion objective, two 100  $\mu$ m adhesive spacers, and finally the coverslip populated by adherent OVCAR-3 cells, resulting in a volume of approximate 5  $\mu$ L in which PBS was initially loaded. The cell to be optically injected was randomly selected from the FOV under DIC. The focal plane, corresponding to the location of the laser trap's focal spot in the Z-axis, was adjusted to correspond with the cell's top surface exposed to freely diffusing liposome suspension. An initial DIC and baseline RhB fluorescent images were acquired on the EMCCD in 16-bit tagged image file format (TIFF). To detect the RhB fluorescence, the following filter cube was used: 545/30 nm excitation filter (HQ545/30 $\times$ ), 570 nm long pass beam splitter (Q570lp), and 610/75 nm emission filter (HQ610/75m) (all from Chroma Technologies Corporation, Bellows Falls, VT). Five microliters of RhB-tagged gold-coated liposomes at a 10 mM lipid concentration was then gently exchanged for the PBS in the cell chamber and optically injected into a single OVCAR-3 cell for 10, 30, 45, 60, 90, or 120 s. Immediately following optical injection, excess RhB-tagged liposomes were gently removed with two PBS washes before

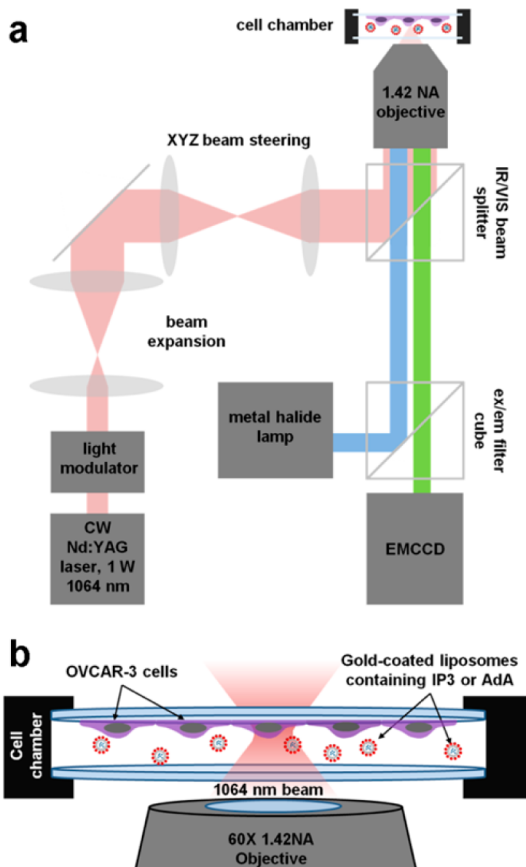


**Figure 9. Optical injection setup.** (a) The schematic depicts the optical setup for the optical trap utilized to inject gold-coated liposomes and fluorescence microscopy. Key components include a CW Nd:YAG 1064 nm trapping laser, a Pockels cell with Glan-laser polarizer to modulate the frequency and pulse width of the laser beam (red), XYZ beam steering, a short-pass 700 nm beam splitter, and a 60 $\times$  1.42 NA objective. To image the cells during optical injection, the beam splitter passes visible light (green), but not the 1064 nm laser, toward the EMCCD allowing for visualization by transmission (i.e., DIC) or epi-fluorescence with a metal halide lamp providing excitation light (blue) and filter cube containing excitation filter, excitation/emission beam splitter, and emission filter. (b) OVCAR-3 cells grown on coverslips are inverted and loaded into a closed cell chamber with gold-coated liposomes for optical injection.

another RhB fluorescence image was acquired. Using ImageJ software (National Institutes of Health, Bethesda, MD), the background fluorescent image was subtracted from the experimental fluorescent images and the total integrated fluorescent intensity originating from the footprint of the injected cell was measured for each.

To quantify the number of gold-coated liposomes injected into a single cell, the integrated fluorescence intensity value measured in the injected cell was divided by the integrated fluorescence intensity originating from single RhB-tagged gold-coated liposome. The latter was determined by diluting liposomes to a 10  $\mu$ M lipid concentration in PBS, loading 5  $\mu$ L of this suspension into a cell chamber absent of cells, and acquiring RhB fluorescence images under the same illumination and camera settings used for imaging RhB fluorescence from the injected cells. Fluorescence images of freely diffusing gold-coated liposomes were analyzed in ImageJ. Ten fluorescent spots in the resulting 16-bit TIFFs, corresponding to 10 individual RhB-tagged gold-coated liposomes, were randomly selected and the integrated fluorescent intensity value for each of the individual liposomes was determined. The average value of

these was assigned as the expected fluorescent intensity contribution from a single injected liposome.

**Optical Injection of IP3 and AdA.** For optical injection experiments, we used gold-coated liposomes containing IP3 or AdA for the purpose of eliciting a  $\text{Ca}^{2+}$  response. Coverslips with OVCAR-3 cells grown to confluence were washed in PBS and incubated with 8  $\mu\text{M}$  Indo-1 AM (Invitrogen, Grand Island, NY), a  $\text{Ca}^{2+}$  sensitive dye, in RPMI medium for 25 min. Indo-1 exhibits peak excitation at 338 nm and has two distinct emission peaks, at 400 and 475 nm, that increase or decrease, respectively, with increasing  $[\text{Ca}^{2+}]$ . The 400 nm Indo-1 emission peak was observed for its greater sensitivity to changes in  $[\text{Ca}^{2+}]$  as compared to the 485 nm emission peak. Following incubation with Indo-1, the coverslips were washed twice in PBS and assembled into the cell chamber, described above, containing 5  $\mu\text{L}$  suspensions of gold-coated liposomes, encapsulating 500  $\mu\text{M}$  IP3, 50  $\mu\text{M}$  AdA, or just PBS, at a 10 mM lipid concentration.

Similar to above, the cell to be optically injected was randomly selected from the FOV under DIC, and the position of the laser's focal spot in the Z-axis was adjusted to correspond with the cell's top surface exposed to freely diffusing liposome suspension. An initial DIC was acquired prior to injection. To detect the Indo-1 400 nm emission, the following optical elements were used: 365/20 nm excitation filter (D365/10 $\times$ , Chroma), 380 nm long pass beam splitter (380dclp, Chroma), and 405/30 nm emission filter (D405/30m, Chroma). Indo-1 fluorescence images were acquired continuously by the EMCCD camera controlled by HClImage Live software (Hamamatsu, Bridgewater, NJ) at a frame rate of 0.25–2 fps before, during, and after optical injection experiments. The experimental sequence for initiating and monitoring  $\text{Ca}^{2+}$  signaling during optical injection was as follows: 30 s of baseline images (representative of  $[\text{Ca}^{2+}]_{\text{baseline}}$  in each cell), 10, 60, or 120 s of images during optical injection, then 30 or 60 s of recovery images after the optical injection beam had been turned off. DIC images were acquired before and after injection experiments for morphological information on the OVCAR-3 cells.

Control experiments were conducted under the same conditions as described above, but instead of suspensions of gold-coated liposomes, either a suspension of uncoated liposomes encapsulating IP3 or PBS with no liposomes was loaded in the cell chamber with the cells, and exposed to the trapping laser for 120 s.

To temporarily block gap junctions between the OVCAR-3 cells, 1 mM octanol in 1 mL PBS was added to the coverslips with cells for 10 min immediately following Indo-1 incubation. Coverslips were washed twice with PBS and loaded into the cell chamber with gold-coated liposomes encapsulating IP3 for optical injection under the same protocol as described above.

Images acquired during optical injection experiments were saved as 16-bit TIFFs for DIC images and multipage TIFFs for Indo-1 fluorescence images and processed using ImageJ software. To determine changes in Indo-1 fluorescence intensity over time in individual cells, the footprint covered by each cell in the experimental FOV was manually outlined and the average fluorescence intensity confined within each cell was calculated for the duration of the experimental image sequence. Average fluorescence intensity was determined for every cell in the FOV beginning with the injected cell, followed by the first group of neighboring cells in direct contact with the injected cells, then the second group of neighboring cells in direct contact with the first group of cells, and so on. Typical experimental FOVs contained between three and six cell groups spanning outward from the injected cell.

To calculate the relative changes in the ratio of  $[\text{Ca}^{2+}] / [\text{Ca}^{2+}]_{\text{baseline}}$  for the duration of the experimental sequence, the average fluorescence intensity for each cell was divided by the average baseline fluorescence intensity, generated from the first 30 s of baseline Indo-1 fluorescence images.

To generate images showing changes in  $[\text{Ca}^{2+}]$ , the first 30 s of baseline Indo-1 fluorescence images were averaged to form a single baseline image. This baseline image was then subtracted from subsequent Indo-1 fluorescence images to highlight cells that were exhibiting increases in cytosolic  $[\text{Ca}^{2+}]$ .

**Conflict of Interest:** The authors declare no competing financial interest.

**Acknowledgment:** This research was supported by NIH (Grants CA120350, CA023074, CA078447, and EB000809) and NSF (Grant CBET 0853921).

**Supporting Information Available:** Supporting Information Movies S1–S8 as described in the text. This material is available free of charge via the Internet at <http://pubs.acs.org>.

## REFERENCES AND NOTES

1. Hanahan, D.; Weinberg, R. A. Hallmarks of Cancer: The Next Generation. *Cell* **2011**, *144*, 646–674.
2. Parrot, J. A.; Nilsson, E.; Mosher, R.; Magrane, G.; Albertson, D.; Pinkel, D.; Gray, J. W.; Skinner, M. K. Stromal-Epithelial Interactions in the Progression of Ovarian Cancer: Influence and Source of Tumor Stromal Cells. *Mol. Cell. Endocrinol.* **2001**, *175*, 29–39.
3. Wong, A. S. T.; Leung, P. C. K. Role of Endocrine and Growth Factors on the Ovarian Surface Epithelium. *J. Obstet. Gynaecol.* **2007**, *33*, 3–16.
4. Ahmed, N.; Thompson, E. W.; Quinn, M. A. Epithelial–Mesenchymal Interconversions in Normal Ovarian Surface Epithelium and Ovarian Carcinomas: an Exception to the Norm. *J. Cell. Physiol.* **2007**, *213*, 581–588.
5. Schauer, I. G.; Sood, A. K.; Mok, S.; Liu, J. Cancer-Associated Fibroblasts and Their Putative Role in Potentiating the Initiation and Development of Epithelial Ovarian Cancer. *Neoplasia* **2011**, *13*, 393–405.
6. Spiller, D. G.; Wood, C. D.; Rand, D. A.; White, M. R. Measurement of Single-Cell Dynamics. *Nature* **2010**, *465*, 736–745.
7. Leybaert, L.; Sanderson, M. J. Intercellular  $\text{Ca}^{2+}$  Waves: Mechanisms and Function. *Physiol. Rev.* **2012**, *92*, 1359–1392.
8. Bendix, P. M.; Oddershede, L. B. Expanding the Optical Trapping Range of Lipid Vesicles to the Nanoscale. *Nano Lett.* **2011**, *11*, 5431–5437.
9. Urban, A. S.; Pfeiffer, T.; Fedoruk, M.; Lutich, A. A.; Feldmann, J. Single-Step Injection of Gold Nanoparticles through Phospholipid Membranes. *ACS Nano* **2011**, *5*, 3585–3590.
10. Stevenson, D. J.; Gunn-Moore, F. J.; Campbell, P.; Dholakia, K. Single Cell Optical Transfection. *J. R. Soc., Interface* **2010**, *7*, 863–871.
11. Troutman, T. S.; Barton, J. K.; Romanowski, M. Biodegradable Plasmon Resonant Nanoshells. *Adv. Mater.* **2008**, *20*, 2604–2608.
12. Leung, S. J.; Romanowski, M. Biomedical Applications: Composite Nanocapsules, Dielectric Properties. *Dekker Encyclopedia of Nanoscience and Nanotechnology*, 3rd ed.; CRC Press: New York, 2014; pp 336–346.
13. Troutman, T. S.; Leung, S. J.; Romanowski, M. Light-Induced Release from Plasmon-Resonant Liposomes. *Adv. Mater.* **2009**, *21*, 2334–2338.
14. Leung, S. J.; Kachur, X. M.; Bobnick, M. C.; Romanowski, M. Wavelength-Selective Light-Induced Release from Plasmon Resonant Liposomes. *Adv. Funct. Mater.* **2011**, *21*, 1113–1121.
15. Leung, S. J.; Romanowski, M. NIR-Activated Content Release from Plasmon Resonant Liposomes for Probing Single-Cell Responses. *ACS Nano* **2012**, *6*, 9383–9391.
16. Leung, S. J.; Romanowski, M. Molecular Catch and Release: Controlled Delivery Using Optical Trapping with Light-Responsive Liposomes. *Adv. Mater.* **2012**, *24*, 6380–6383.
17. Berridge, M. J.; Taylor, C. W. Inositol Triphosphate and Calcium Signaling. *Cold Spring Harb Symp. Quant. Biol.* **1988**, *53*, 927–933.
18. Berridge, M. J.; Irvine, R. F. Inositol Phosphates and Cell Signalling. *Nature* **1989**, *341*, 197–205.
19. Berridge, M. J.; Bootman, M. D.; Lipp, P. Calcium – a Life and Death Signal. *Nature* **1998**, *395*, 645–648.
20. Berridge, M. J.; Lipp, P.; Bootman, M. D. The Versatility and Universality of Calcium Signaling. *Nat. Rev. Mol. Cell Biol.* **2000**, *1*, 11–21.

21. Saleem, H.; Tovey, S. C.; Rahman, T.; Riley, A. M.; Potter, B. V.; Taylor, C. W. Stimulation of Inositol 1, 4, 5-Trisphosphate (IP<sub>3</sub>) Receptor Subtypes by Analogues of IP<sub>3</sub>. *PLoS One* **2013**, *8*, e54877.
22. Blatter, L. A.; Wier, W. G. Intracellular Diffusion, Binding, and Compartmentalization of the Fluorescent Calcium Indicators Indo-1 and Fura-2. *Biophys. J.* **1990**, *58*, 1491–1499.
23. Finch, E. A.; Turner, T. J.; Goldin, S. M. Calcium as a Coagonist of Inositol 1,4,5-Trisphosphate-Induced Calcium Release. *Science* **1991**, *252*, 443–446.
24. Lin, J. H.; Weigel, H.; Cotrina, M. L.; Liu, S.; Bueno, E.; Hansen, A. J.; Goldman, S.; Nedergaard, M. Gap-Junction-Mediated Propagation and Amplification of Cell Injury. *Nat. Neurosci.* **1998**, *1*, 494–500.
25. Nihei, O. K.; Campos de Carvalho, A. C.; Spray, D. C.; Savino, W.; Alves, L. A. A Novel Form of Cellular Communication among Thymic Epithelial Cells: Intercellular Calcium Wave Propagation. *Am. J. Physiol.* **2003**, *285*, C1304–C1313.
26. Sanderson, M. J.; Charles, A. C.; Dirksen, E. R. Mechanical Stimulation and Intercellular Communication Increases Intracellular Ca<sup>2+</sup> in Epithelial Cells. *Cell Regul.* **1990**, *1*, 585–596.
27. Isakson, B. E.; Seedorf, G. J.; Lubman, R. L.; Evans, W. H.; Boitano, S. Cell–Cell Communication in Heterocellular Cultures of Alveolar Epithelial Cells. *Am. J. Resp. Cell Mol.* **2003**, *29*, 552–561.
28. Whitaker, M.; Irvine, R. F. Inositol 1,4,5-Trisphosphate Microinjection Activates Sea Urchin Eggs. *Nature* **1984**, *312*, 636–639.
29. Churchill, G.; Louis, C. Roles of Ca<sup>2+</sup>, Inositol Trisphosphate and Cyclic ADP-Ribose in Mediating Intercellular Ca<sup>2+</sup> Signaling in Sheep Lens Cells. *J. Cell Sci.* **1998**, *111*, 1217–1225.
30. Soughayer, J. S.; Krasieva, T.; Jacobson, S. C.; Ramsey, J. M.; Tromberg, B. J.; Allbritton, N. L. Characterization of Cellular Optoporation with Distance. *Anal. Chem.* **2000**, *72*, 1342–1347.
31. Yi, C.; Li, C. W.; Ji, S.; Yang, M. Microfluidics Technology for Manipulation and Analysis of Biological Cells. *Anal. Chim. Acta* **2006**, *560*, 1–23.
32. Leybaert, L.; Sanderson, M. J. Intercellular Calcium Signaling and Flash Photolysis of Caged Compounds. In *Methods in Molecular Biology: Connexin Methods and Protocols*; Bruzzone, R., Giaume, C., Eds.; Humana Press: Totowa, NJ; 2001; Vol. 154, pp 407–430.
33. Sun, B.; Chiu, D. T. Spatially and Temporally Resolved Delivery of Stimuli to Single Cells. *J. Am. Chem. Soc.* **2003**, *125*, 3702–3703.
34. Kantevari, S.; Hoang, C. J.; Ogrordnik, J.; Egger, M.; Niggli, E.; Ellis-Davies, G. C. Synthesis and Two-Photon Photolysis of 6-(Ortho-Nitroveratryl)-Caged IP<sub>3</sub> in Living Cells. *Chem-BioChem* **2006**, *7*, 174–180.
35. Ellis-Davies, G. C. R. Caged Compounds: Photorelease Technology for Control of Cellular Chemistry and Physiology. *Nat. Methods* **2007**, *4*, 619–628.
36. Gu, L.; Mohanty, S. K. Targeted Microinjection Into Cells and Retina Using Optoporation. *J. Biomed. Opt.* **2011**, *16*, 128003–1280036.
37. Akl, H.; Bultynck, G. Altered Ca<sup>2+</sup> Signaling in Cancer Cells: Proto-Oncogenes and Tumor Suppressors Targeting IP<sub>3</sub> Receptors. *Biochim. Biophys. Acta Rev. Cancer* **2013**, *1835*, 180–193.
38. Stephens, L.; Anderson, K.; Stokoe, D.; Erdjument-Bromage, H.; Painter, G. F.; Holmes, A. B.; Gaffney, P. R. J.; Reese, C. B.; McCormick, F.; Tempst, P.; et al. Protein Kinase B Kinases that Mediate Phosphatidylinositol 3, 4, 5-Trisphosphate-Dependent Activation of Protein Kinase B. *Science* **1998**, *279*, 710–714.
39. Giorgi, C.; Ito, K.; Lin, H. K.; Santangelo, C.; Wieckowski, M. R.; Lebiedzinska, M.; Bononi, A.; Bonora, M.; Duszynski, J.; Bernardi, R.; et al. PML Regulates Apoptosis at Endoplasmic Reticulum by Modulating Calcium Release. *Science* **2010**, *330*, 1247–1251.
40. Braun, G. B.; Pallaoro, A.; Wu, G.; Missirlis, D.; Zasadzinski, J. A.; Tirrell, M.; Reich, N. O. Laser-Activated Gene Silencing via Gold Nanoshell–siRNA Conjugates. *ACS Nano* **2009**, *3*, 2007–2015.
41. Anderson, L. J.; Hansen, E.; Lukianova-Hleb, E. Y.; Hafner, J. H.; Lapotko, D. O. Optically Guided Controlled Release from Liposomes with Tunable Plasmonic Nanobubbles. *J. Controlled Release* **2010**, *144*, 151–158.
42. Lukianova-Hleb, E. Y.; Belyanin, A.; Kashinath, S.; Wu, X.; Lapotko, D. O. Plasmonic Nanobubble-Enhanced Endosomal Escape Processes for Selective and Guided Intracellular Delivery of Chemotherapy to Drug-Resistant Cancer Cells. *Biomaterials* **2012**, *33*, 1821–1826.
43. Gregersen, K. A.; Hill, Z. B.; Gadd, J. C.; Fujimoto, B. S.; Maly, D. J.; Chiu, D. T. Intracellular Delivery of Bioactive Molecules Using Light-Addressable Nanocapsules. *ACS Nano* **2010**, *4*, 7603–7611.
44. Slack, M. D.; Martinez, E. D.; Wu, L. F.; Altschuler, S. J. Characterizing Heterogeneous Cellular Responses to Perturbations. *Proc. Natl. Acad. Sci. U.S.A.* **2008**, *105*, 19306–19311.
45. Altschuler, S. J.; Wu, L. F. Cellular Heterogeneity: Do Differences Make a Difference? *Cell* **2010**, *141*, 559–563.
46. Woodward, T. L.; Sia, M. A.; Blaschuk, O. W.; Turner, J. D.; Laird, D. W. Deficient Epithelial-Fibroblast Heterocellular Gap Junction Communication can be Overcome by Co-Culture with an Intermediate Cell Type but Not by E-Cadherin Transgene Expression. *J. Cell Sci.* **1998**, *111*, 3529–3539.
47. Needham, D.; Anyarambhatla, G.; Kong, G.; Dewhurst, M. W. A New Temperature-Sensitive Liposome for Use with Mild Hyperthermia: Characterization and Testing in a Human Tumor Xenograft Model. *Cancer Res.* **2000**, *60*, 1197–1201.